ChemComm

COMMUNICATION

View Article Online
View Journal | View Issue

Cite this: *Chem. Commun.*, 2025, **61**, 1641

Received 26th August 2024,
Accepted 2nd December 2024

DOI: 10.1039/d4cc04370g

rsc.li/chemcomm

Post-synthetic modification of amine-functionalized permanently porous coordination cages†

Jahidul Hoq,[a] Michael R. Dworzak,[b] Duleeka Dissanayake,[a] Rebecca X. Skalla,[a] Nobuyuki Yamamoto,[a] Glenn P. A. Yap[b] and Eric D. Bloch*[a]

This manuscript explores the post-synthetic modification (PSM) of amine-functionalized porous coordination cages, specifically focusing on the formation of imine bonds through reactions with aldehydes. Targeting various cage topologies, including zirconium-, magnesium-, and molybdenum-based structures, we demonstrate the tunability of cage solubility and porosity through selective functionalization where the proximity of amine groups on the parent cage impacts the extent of modification. The work highlights the reversible nature of imine formation, offering potential applications in solubility switching and mixed-metal solid synthesis.

Over the past decade, as their permanent porosity in the solid state has been developed and improved, transition metal-based supramolecular species have gained considerable attention as solid adsorbent materials.[1–4] This permanent porosity in the solid state distinguishes them from the broader class of cage molecules, and as such, they are typically referred to as porous coordination cages,[5] metal–organic supercontainers,[6] or metal–organic polyhedra (MOPs).[7] It is no coincidence that this latter term has parallels to the broad class of permanently porous, three-dimensional solids known as metal–organic frameworks (MOFs).[8] Beyond just the name alone, these molecular adsorbents share many properties with MOFs.[9,10] Structurally, both solids are generally composed of divalent or trivalent first-row transition metal cations and weak-field anionic bridging ligands.[11,12] However, as both areas have progressed, their chemistry has dramatically expanded in terms of both inorganic and organic components. Tunability at both of these units has afforded an incredible diversity of structures in both MOFs and porous coordination cages, leading to exhaustive investigations across various fields.[13,14]

The structural stability of porous metal–organic materials has also allowed for the diversification of their structures, properties, and performance *via* post-synthetic modification.[15–17] Both MOFs and MOPs can be modified to incorporate functional groups that may not be compatible with their assembly conditions or require specific spatial orientation that would not be possible during direct assembly.[18] Post-synthetic modification strategies for MOFs are quite mature, and several reviews detail this exciting chemistry in great detail.[19–21] Given their compositional and structural similarities, MOPs have also been shown to be compatible with post-synthetic modification chemistry.[22] Inspiring prior work has shown that modifications to the exterior or interior surfaces of coordination cages can be used to tune their properties. A wealth of work has been done here, detailing alkylation,[23] acylation,[24] cross-coupling,[25] dehydration,[26] condensation,[27] click,[28] and polymerization reactions,[29] among many others.

We have been particularly interested in a subset of these modification reactions, as they can show reversibility. For example, we have previously shown that anion binding can be used to impart solubility to otherwise insoluble coordination cages.[30] Condensation reactions may also prove versatile for these types of modifications. The reaction of an amine with an aldehyde produces an imine with concomitant water production.[31,32] The other Bloch group working in this area has shown the utility of the amine-to-imine reaction to great effect, where they have used it to tether cages in the solution state in direct covalent crosslinking of cages.[33] In the work detailed here, we highlight an extension of this approach for a subset of amine-functionalized permanently porous coordination cages featuring amine-based isophthalic acid or terephthalic acid ligands. We show that for a set of aldehyde-containing molecules, a molybdenum-based cuboctahedral coordination cage can be fully functionalized to impart tunable solubility or install metal-binding groups to create mixed-metal solids.

In targeting $-NH_2$ functionalized cages for post-synthetic modification to imine groups, we investigated a variety of cage

[a] *Department of Chemistry, Indiana University, Bloomington, Indiana 47405, USA. E-mail: edbloch@iu.edu*
[b] *Department of Chemistry & Biochemistry, University of Delaware, Newark, Delaware 19716, USA*

† Electronic supplementary information (ESI) available: Adsorption isotherms, crystallographic information, spectroscopic data. CCDC 2379514 and 2378545. For ESI and crystallographic data in CIF or other electronic format see DOI: https://doi.org/10.1039/d4cc04370g

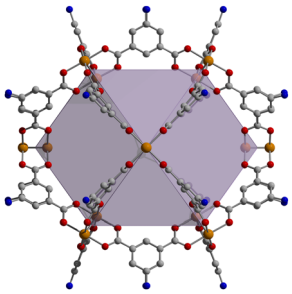

Fig. 1 Structure of the cuboctahedral $Mo_{24}(5\text{-}NH_2\text{-}bdc)_{24}$ cage where orange, red, gray, and blue spheres represent molybdenum, oxygen, carbon, and nitrogen, respectively. Hydrogen atoms and metal-coordinated solvent molecules have been omitted for clarity.

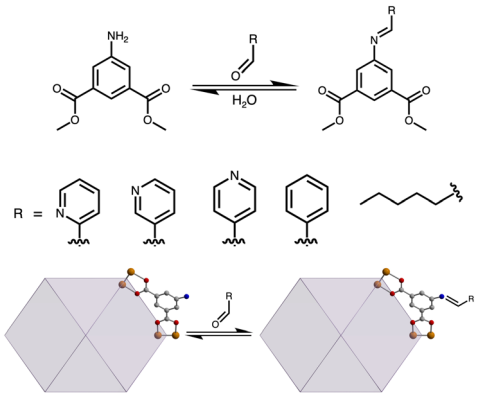

Fig. 2 Aldehydes utilized in studying the reactivity toward imine functionalization of dimethyl-5-NH_2-bdc and a schematic of $Mo_{24}(5\text{-}NH_2\text{-}bdc)_{24}$ undergoing imine functionalization with corresponding aldehydes. R-CHO, left to right, 2-formylpyridine, 3-formylpyridine, 4-formyl pyridine, benzaldehyde, and hexanal.

topologies. In this regard, both 2-aminoterephthalic acid and 5-aminoisophthalic acid containing structures are viable. Although a number of various cage structure types are compatible with these types of ligands, we investigated three different cage topologies, including zirconocene-based $[Zr_{12}(\mu_3\text{-}O)_4(\mu_2\text{-}OH)_{12}(Cp)_{12}(2\text{-}NH_2\text{-}bdc)_6]^{4+}$, calixarene-capped $[(Mg_4SC4A)_4(\mu_4\text{-}OH)_4(5\text{-}NH_2\text{-}bdc)_8]^{4-}$, and molybdenum paddlewheel-based $Mo_{24}(5\text{-}NH_2\text{-}bdc)_{24}$ structures (ESI,† Fig. S1 and Fig. 1) given their previously established compatibility with post-synthetic modification strategies.[11,12] The syntheses of these cages have been reported and are generally straightforward involving the solvothermal reaction of appropriate metal salts and ligands at elevated temperatures.[34] Although the cage materials are products of amide-based syntheses, activated samples are obtained by washing the as-synthesized materials with $CHCl_3$, MeOH, and THF respectively, and activating under dynamic vacuum. All three structures are porous to CO_2 with BET (Langmuir) surface areas of 385 (802), 262 (708), and 938 (1452) $m^2\ g^{-1}$ (ESI,† Fig. S2–S4) for $[Zr_{12}(\mu_3\text{-}O)_4(\mu_2\text{-}OH)_{12}(Cp)_{12}(2\text{-}NH_2\text{-}bdc)_6]^{4+}$, $[(Mg_4SC4A)_4(\mu_4\text{-}OH)_4(5\text{-}NH_2\text{-}bdc)_8]^{4-}$, and $Mo_{24}(5\text{-}NH_2\text{-}bdc)_{24}$, respectively.

The heterogeneous reaction of amine-functionalized cages with excess 2-formylpyridine in THF for two days affords solids with modest solubility in polar organic solvents such as DMF and DMSO. IR spectra of isolated solids confirm imine formation with the emergence of a feature associated with an N=C stretch in the range of 1645–1655 cm^{-1} (ESI,† Fig. S41(d) and (e)) while DOSY NMR confirms the solution persistence of the magnesium- and molybdenum-based cages (Fig. S30, ESI†) and mass spectrometry shows the zirconium-based cage remains intact after functionalization. Thorough solvent exchange and activation at the appropriate temperatures affords samples with BET (Langmuir) surface areas of 218 (511), 190 (489) and 97 (221) $m^2\ g^{-1}$ (ESI,† Fig. S5–S7) for $[Zr_{12}(\mu_3\text{-}O)_4(\mu_2\text{-}OH)_{12}(Cp)_{12}(2\text{-}pyridineimine\text{-}bdc)_6]^{4+}$, $[(Mg_4SC4A)_4(\mu_4\text{-}OH)_4(2\text{-}pyridineimine\text{-}bdc)_8]^{4-}$, and $Mo_{24}(2\text{-}pyridineimine\text{-}bdc)_{24}$, respectively. Although the zirconium-based cage and $Mo_{24}(5\text{-}NH_2\text{-}bdc)_{24}$ have modest solubility in DMSO, all samples were digested to facilitate NMR to quantify the extent of reaction of the amine functional group with the target aldehyde to give imine-functionalized cages (ESI,† Fig. S8, S10 and S13).

To further assess the reactivity of $Mo_{24}(5\text{-}NH_2\text{-}bdc)_{24}$ with various aldehydes, we increased the substrate scope to include 3-formylpyridine, 4-formylpyridine, benzaldehyde, and hexanal (Fig. 2). Initial reactions of these substrates with cage in THF for 24 hours afforded products with varying levels of conversion presumably implying varying degrees of reactivity of the aldehydes. The kinetics of these types of reactions have been exhaustively studied by Anslyn and coworkers where they have also investigated the equilibrium between imine and aminal formation using a range of aromatic amines with *para*- and *meta*-substitutions in conjunction with 2-formylpyridine.[35] They have shown that enhanced nucleophilicity of the amine group, which is typically associated with electron-donating groups, promotes imine formation, whereas electron-withdrawing groups tend to favor aminal product, particularly in the presence of zinc triflate.

To understand the relative reactivity of the substrates employed here, we undertook a systematic approach targeted at relative reaction rates and conversion for the aforementioned aldehydes. Using the dimethyl ester of the ligand as an easy to characterize cage surrogate, a series of homogeneous THF solutions of dimethyl-5-NH_2-bdc and five equivalents of aldehyde were prepared in THF and monitored by ^1H NMR spectroscopy. Spectra were recorded after 2, 4, 20, and 38 hours of reaction time to monitor the formation of imine complexes relative to the total amine present, (ESI,† Fig. S14–S17). After 2 hours, we observed 74, 51, 12, and 3% conversion for 4-formylpyridine, 2-formylpyridine, 3-formylpyridine, and benzaldehyde, respectively (ESI,† Fig. S19). After four hours, these values increased to 92, 53, 25, and 10%, respectively. After 38 hours of total reaction time, the conversion of amine-based ligand to imine-functionalized product 94, 54, 78, and 24% for 4-formylpyridine, 2-formylpyridine, 3-formylpyridine, and benzaldehyde. These results are in general agreement with those observed for analogous imine-forming reactions. It is of note that we observed marked differences in not only apparent reaction rates but in reaction equilibria as well. As a condensation reaction, amine-imine equilibrium is sensitive to water content in the reaction medium. To probe this further, a drop of water was added to each reaction tube and ^1H NMR spectra

were recorded after 24 hours. The analysis revealed that the added water shifted the equilibrium and decreased the total imine content to 81, 38, 56, and 18% for 4-formylpyridine, 2-formylpyridine, 3-formylpyridine, and benzaldehyde (ESI,† Fig. S14–S17). After an additional 24 hours, we observed no further change in product distribution.

Given a better understanding of the relatively sluggish reaction rates for specific aldehyde reagents, we screened further reactivity of Mo_{24}(5-NH_2-bdc)$_{24}$ with 4-formylpyridine, 3-formylpyridine, 2-formylpyridine, benzaldehyde, and hexanal. Due to solubility constraints, the functionalization of the cage remains largely heterogeneous. Accordingly, Mo_{24}(5-NH_2-bdc)$_{24}$ was suspended in THF in the presence of excess aldehyde and allowed to stir for 2 days at RT. During this time, we observed partial solubilization of the benzaldehyde and hexanal-functionalized cages. After 2 days, the residual solid was isolated *via* centrifugation and washed with dichloromethane five times over the course of three days to remove unreacted aldehyde. Functionalized cages were then vacuum dried and analyzed by ^{1}H NMR, IR, and UV-vis spectroscopies. DOSY NMR confirmed the persistence of the cages after functionalization (Fig. S30, ESI†) while NMR spectra of digested samples, where the imine is hydrolyzed back to aldehyde and amine, confirmed the expected stoichiometry (ESI,† Fig. S13 and S20–S23). Additionally, solution state UV-vis spectra reveal maximum absorbances at 467 nm for all five products (ESI,† Fig. S31 and S32), which is identical to the value for the starting cage and confirms the persistence of the Mo–Mo paddlewheel unit (Fig. 4, orange). This was expected given the stability of this structural unit to even harsh modification conditions. Furthermore, potential covalent-coordination of aldehydic species at the open metal site of the paddlewheel was ruled out by utilizing an isostructural non-amine cage, Mo_{24}(*m*-bdc)$_{24}$ (ESI,† Fig. S30(b)). Gas adsorption analysis was performed to confirm the retention of porous structure, albeit with reduced surface area as the cages display decreased BET surface areas of 97, 94, 116, 356, and 144 m^2 g^{-1} for Mo_{24}(2-pyridineimine-bdc)$_{24}$, Mo_{24}(3-pyridineimine-bdc)$_{24}$, Mo_{24}(4-pyridineimine-bdc)$_{24}$, Mo_{24}(2-benzalimine-bdc)$_{24}$, and Mo_{24}(hex-imine-bdc)$_{24}$, respectively as determined by 195 K CO_2 adsorption isotherms (ESI,† Fig. S7).

Mo_{24}(benzalimine-bdc)$_{24}$ and Mo_{24}(hex-imine-bdc)$_{24}$ showed moderate solubility in a variety of organic solvents, including THF (ESI,† Fig. S24), benzene (ESI,† Fig. S42), and acetone. It was generally observed that the rate of solubilization tracked with the rate of imine formation. In order to more closely monitor this, we suspended Mo_{24}(5-NH_2-bdc)$_{24}$ in THF, added excess aldehyde, and monitored the absorbance of the resulting solution over the course of approximately 8 hours. As shown in Fig. 3 for the reaction of Mo_{24}(5-NH_2-bdc)$_{24}$ with benzaldehyde, appreciable cage solubility is observed after just two hours and continually increases over the course of 8 hours until reaching apparent solution saturation. Similar reactivity and solubility increases are observed for the hexane-functionalized cage (ESI,† Fig. S33). A distinct benefit of imine-functionalization is the reversibility of the amine to imine reaction in the presence of water. Upon adding degassed water to Mo_{24}(benzalimine-bdc)$_{24}$, we observed precipitation of the

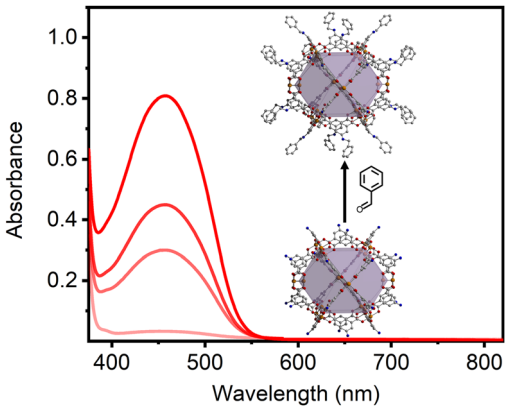

Fig. 3 Reaction of Mo_{24}(5-NH_2-bdc)$_{24}$ with benzaldehyde over the course of four hours with absorbance at 467 nm of 0.03, 0.29, 0.43, 0.79 at 1, 2, 3, and 4, hours, respectively.

THF-insoluble amine-functionalized cage, along with the presence of free aldehyde in THF (ESI,† Fig. S24 and S25). For the cage treated with DCl, free aldehyde was detected only under mildly acidic conditions (ESI,† Fig. S22) and remained largely undetected as -CDO under more strongly acidic conditions (ESI,† Fig. S8, S10, S13, S20 and S21).

The solubility of the pyridine-functionalized cages remains limited to DMF and DMSO but may offer the advantage of metallation at the external surface of the cage. Specifically, the 2-pyridineimine site is the most structurally conducive to metal coordination and has previously shown utility for the preparation of mixed-metal MOFs.[36] As such, we targeted postsynthetic metallation of Mo_{24}(2-pyridineimine-bdc)$_{24}$. Heterogeneous metallation of the cage sample proceeded by soaking the solid sample in metal ion solutions where anhydrous $CoCl_2$ or [(*S*)-(−)2,2′-bis (diphenylphosphino)-1,1′-binaphthyl]-diaquo-palladium(II) triflate; $Pd(OTf)_2$] was dissolved in THF. The metallation with $Pd(OTf)_2$ afforded $Pd(OTf)_2$@Mo_{24}(2-pyridineimine-bdc)$_{24}$ cage which was initially detected *via* ^{19}F NMR (ESI,† Fig. S26) and ^{31}P NMR (ESI,† Fig. S27), with further confirmation provided by UV-vis

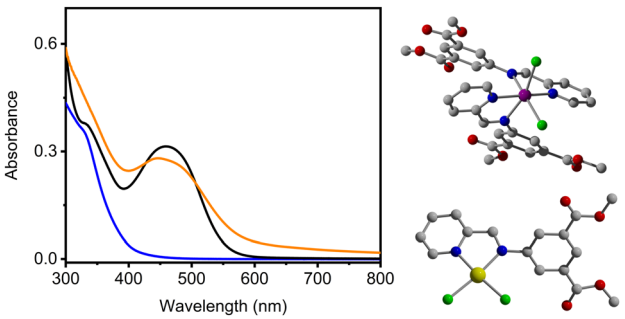

Fig. 4 Single crystal structures of dimethyl-2-pyridineimine-bdc metallated with $CoCl_2$, (top right) or $PdCl_2$ (bottom right) where yellow, purple, red, gray, green, and blue spheres represent palladium, cobalt, oxygen, carbon, chlorine, and nitrogen atoms respectively. The UV-vis spectrum (Left) of $Pd(OTf)_2$@Mo_{24}(2-pyridineimine-bdc)$_{24}$, cage (black) in DMSO displays absorbances present in the Mo_{24}(5-NH_2-bdc)$_{24}$ (orange) cage and the $Pd(OTf)_2$ metallated dimethyl-2-pyridineimine-bdc ligand (blue).

spectroscopy showing a characteristic $Pd(OTf)_2$ absorbance (Fig. 4 (left), black) that was compared to a metallated ligand analog of the material (Fig. 4 (left), blue). Metallation with $PdCl_2$ yielded a structure (Fig. 4, bottom right) with cis-Cl square planar geometry at the chelate site of dimethyl-2-pyridineimine-bdc. The UV-vis absorbance of $PdCl_2$@dimethyl-2-pyridineimine-bdc is comparable to $Pd(OTf)_2$@dimethyl-2-pyridineimine-bdc (ESI,† Fig. S34).

Mo_{24}(2-pyridineimine-bdc)$_{24}$ becomes insoluble upon $CoCl_2$ metallation, limiting optical comparison to solid-state absorbance measurements with $CoCl_2$-metallated dimethyl ligand analogs, which were structurally characterized by single crystal X-ray diffraction (Fig. 4, top right). $CoCl_2$ metallation into Mo_{24}(2-pyridineimine-bdc)$_{24}$ was monitored by UV-vis (ESI,† Fig. S37). X-ray photoelectron spectroscopy (XPS) analysis further confirmed metallation and the presence of all elements in the expected ratios within the metallated cages (ESI,† Fig. S39 and S40).

In conclusion, this study demonstrates the versatility and potential of post-synthetic modification (PSM) strategies for tailoring the properties of amine-functionalized porous coordination cages. By exploring various cage topologies and their reactivity with different aldehydes, we have shown that imine formation can significantly influence both the solubility and porosity of these materials. The reversible nature of the amine-to-imine transformation offers a promising approach for dynamic control over cage properties, including solubility switching and metal-binding capabilities.

The authors gratefully acknowledge financial support from the National Science Foundation (2154976) and Indiana University. Support for the acquisition of the Bruker Venture D8 diffractometer through the Major Scientific Research Equipment Fund from the President of Indiana University and the Office of the Vice President for Research is gratefully acknowledged. GPAY thanks the National institutes of Health for grant S10 OD026896A.

Data availability

The data supporting this article have been included as part of the ESI.† Crystallographic data for $PdCl_2$@dimethyl-2-pyridineimine-bdc and $CoCl_2$@dimethyl-2-pyridineimine-bdc have been deposited at the CCDC with numbers 2379514 and 2378545, respectively.

Conflicts of interest

There are no conflicts to declare.

References

1 M. M. Deegan, M. R. Dworzak, A. J. Gosselin, K. J. Korman and E. D. Bloch, *Chem. – Eur. J.*, 2021, **27**, 4531.
2 A. J. Gosselin, C. A. Rowland and E. D. Bloch, *Chem. Rev.*, 2020, **120**(16), 8987–9014.
3 G. R. Lorzing, A. J. Gosselin, B. S. Lindner, R. Bhattacharjee, G. P. A. Yap, S. Caratzoulas and E. D. Bloch, *Chem. Commun.*, 2019, **55**, 9527–9530.
4 B. Lee, I.-H. Park and J. Park, *ACS Mater. Lett.*, 2022, **4**(11), 2388–2393.
5 X. Z. Li, C. B. Tian and Q. F. Sun, *Chem. Rev.*, 2022, **122**, 6374–6458.
6 F.-R. Dai and Z. Wang, *J. Am. Chem. Soc.*, 2012, **134**(19), 8002–8005.
7 S. Lee, H. Jeong, D. Nam, M. S. Lah and W. Choe, *Chem. Soc. Rev.*, 2021, **50**, 528–555.
8 H.-C. Zhou, J. R. Long and O. M. Yaghi, *Chem. Rev.*, 2012, **112**(2), 673–674.
9 B. S. Pilgrim and N. R. Champness, *ChemPlusChem*, 2020, **85**, 1842.
10 M.-H. Yu, P. Zhang, R. Feng, Z.-Q. Yao, Y.-C. Yu, T.-L. Hu and X.-H. Bu, *ACS Appl. Mater. Interfaces*, 2017, **9**(31), 26177–26183.
11 M. M. Deegan, A. M. Antonio, G. A. Taggart and E. D. Bloch, *Coord. Chem. Rev.*, 2021, **430**, 213679.
12 A. Dey, M. R. Dworzak, K. D. P. Korathotage, M. Ghosh, J. Hoq, C. M. Montone, G. P. A. Yap and E. D. Bloch, *Dalton Trans.*, 2024, **53**, 4005–4009.
13 M. Wu, G. Lin, R. Li, X. Liu, S. Liu, J. Zhao and W. Xie, *Sci. Adv.*, 2024, **10**(19), eadl4449.
14 T. Goculdas, K. Korathotage, C. Montone, S. Sadula, E. D. Bloch and D. G. Vlachos, *ACS Appl. Mater. Interfaces*, 2023, **15**(49), 57070–57078.
15 J. Liu, Z. Wang, P. Cheng, M. J. Zaworotko, Y. Chen and E. Z. Zhang, *Nat. Cem. Rev.*, 2022, **6**, 339–356.
16 M. R. Dworzak, J. Sampson, C. M. Montone, K. J. Korman, G. P. A. Yap and E. D. Bloch, *Chem. Mater.*, 2024, **36**(2), 752–758.
17 G. A. Taggart, A. M. Antonio, G. R. Lorzing, G. P. A. Yap and E. D. Bloch, *ACS Appl. Mater. Interfaces*, 2020, **12**(22), 24913–24919.
18 M. Kalaj and S. M. Cohen, *ACS Cent. Sci.*, 2020, **6**(7), 1046–1057.
19 Z. Wang and S. M. Cohen, *Chem. Soc. Rev.*, 2009, **38**, 1315–1329.
20 W. He, D. Lv, Y. Guan and S. Yu, *J. Mater. Chem. A*, 2023, **11**, 24519–24550.
21 W. M. Bloch, A. Burgun, C. J. Doonan and C. J. Sumby, *Chem. Commun.*, 2015, **51**, 5486–5489.
22 D. Luo, X.-W. Zhu, X.-P. Zhou and D. Li, *Chem. – Eur. J.*, 2024, **30**, e202400020.
23 J. Hoq and E. D. Bloch, *Chem. Commun.*, 2024, **60**, 6945–6948.
24 A. Carne-Sanchez, J. Albalad, T. Grancha, I. Imaz, J. Juanhuix, P. Larpent, S. Furukawa and D. Maspoch, *J. Am. Chem. Soc.*, 2019, **141**(9), 4094–4102.
25 D. Nam, J. Huh, J. Lee, J. H. Kwak, H. Y. Jeong, K. Choi and W. Choe, *Chem. Sci.*, 2017, **8**, 7765–7771.
26 H. Wang, Y. Jin, N. Sun, W. Zhang and J. Jiang, *Chem. Soc. Rev.*, 2021, **50**, 8874–8886.
27 M. L. Schneider, A. W. Markwell-Heys, O. M. Linder-Patton and W. M. Bloch, *Front. Chem.*, 2021, **9**, 696081.
28 M. R. Dworzak, C. M. Montone, N. I. Halaszynski, G. P. A. Yap, C. J. Kloxin and E. D. Bloch, *Chem. Commun.*, 2023, **59**, 8977–8980.
29 D. Nam, J. Huh, J. Lee, J. H. Kwak, H. Y. Jeong, K. Choi and W. Choe, *Chem. Sci.*, 2017, **8**, 7765–7771.
30 A. M. Antonio, M. R. Dworzak, K. J. Korman, G. P. A. Yap and E. D. Bloch, *Chem. Mater.*, 2022, **34**(24), 10823–10831.
31 A. Khobotov-Bakishev, P. Samanta, K. Roztocki, J. Albalad, S. Royuela, S. Furukawa, F. Zamora, A. Carne-Sanchez and D. Maspoch, *Adv. Func. Mater.*, 2024, **34**, 2312166.
32 W. M. Bloch, R. Babarao and M. L. Schneider, *Chem. Sci.*, 2020, **11**, 3664–3671.
33 M. L. Schneider, J. A. Campbell, A. D. Slattery and W. M. Bloch, *Chem. Commun.*, 2022, **58**, 12122–12125.
34 G. R. Lorzing, A. J. Gosselin, B. A. Trump, A. H. P. York, A. Sturluson, C. A. Rowland, G. P. A. Yap, C. M. Brown, C. M. Simon and E. D. Bloch, *J. Am. Chem. Soc.*, 2019, **141**(30), 12128–12138.
35 Y. Zhou, Y. Yuan, L. You and E. V. Anslyn, *Chem. – Eur. J.*, 2015, **21**(22), 8207–8213.
36 C. J. Doonan, W. Morris, H. Furukawa and O. M. Yaghi, *J. Am. Chem. Soc.*, 2009, **131**(27), 9492–9493.

